Design and analysis of ripple-based controllers for buck converters based on discrete modeling and Floquet theory

Jorge Cortés, Vladimir Šviković, Pedro Alou, Jesús A. Oliver and José A. Cobos

I. Introduction

V^2I_c [1] (fig.1) is a ripple-based control that presents a very fast dynamic response under load steps and voltage reference steps. It is composed by a slow loop where the output voltage is regulated with a linear controller and a fast loop where the error of the output voltage and the current through the output capacitor are added and act as the triangular signal for the modulator. A compensating ramp can be added in order to improve the stability of the system.

The current through the output capacitor is sensed indirectly with a trans-impedance amplifier [2] which, for analysis purposes, is equivalent to a RLC network (fig. 2). If the gain and phase of the RLC network is proportional to the gain and phase of the output capacitor, then the current through the RLC network will mirror the current through the output capacitor with a certain gain. A mismatch in the gain or phase will provoke a distorted measurement of the current and, since it is a ripple-based control that uses it as a triangular control signal, it may eventually induce sub-harmonics oscillations in the system. For this reason, V^2I_c control needs to be robust against variation in the parasitic ESR and ESL of the output capacitor. The compensating ramp, the gain of the current sensor and the gain of the error voltage of the fast loop are design parameters to help maintain stability over the desired operation range of the duty cycle while achieving a fast dynamic response.

The goal of this paper is to model a closed-loop V^2I_c control considering the ESR and the ESL of the output capacitor and the equivalent RLC network and analyze its stability to carry out sensitivity analysis regarding critical parameters to ensure a robust operation.

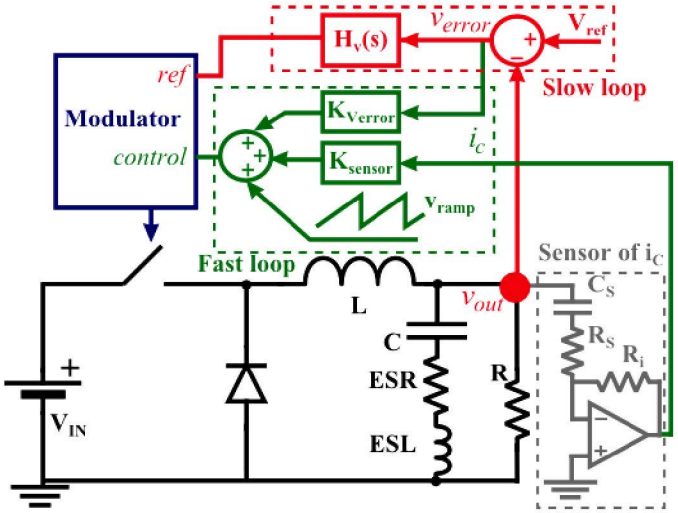

Fig. 1: V^2I_c, a ripple-based controller.

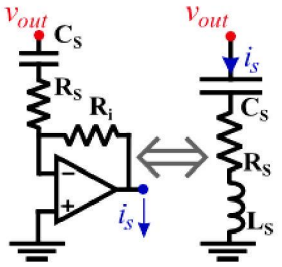

Fig. 2: The current sensor behaves like a RLC network.

This work has been partially supported by Spanish Government Innovation and Science Office (MCINN), under research grant no. DPI- 2010-20096, "FAST" project.

This work has been partially supported by EU FP7-ICT-2011-8 – Power-SWIPE – Project no.: 318529

II. Review of alternatives

In the scientific literature, there are several approaches to derive models of power converter that can predict sub-harmonic oscillations, mostly applied to common control techniques. Tan and Middlebrook [3] and Tang et al. [4] proposed a model for the peak current mode and the average current model control, respectively, both based on the modeling of the modulation stage. Li and Lee [5] employed the Describing Function technique (DF) to model as an unified system a V^2 constant on-time control. These techniques provide a control-to-output and output impedance transfer function in symbolic form from which an open-loop stability criterion, an study of the movement of poles and zeros [6, 7] and an equivalent circuit model [8] can be derived. The DF technique achieves an excellent modeling of the V^2-controlled buck converter and it is up to now the best tool to understand the behavior of the system. However, it may fall short for more complex ripple-based controllers such as $V^2 I_c$ control where a great number of state variables needs to be taken into account, not only the inductor current and the voltage in the output capacitor. Also, for very high switching converters, the ripple of the output voltage caused by the ESL can be dominant and, thus, it needs to be included in the modeling, increasing again the complexity by adding another state variable.

In the 90s, the sub-harmonic oscillations started to be studied from the point of view of bifurcation phenomena. The sub-harmonic oscillation can be predicted by means of the Floquet theory that, for a T-periodic system, establishes whether a perturbation will grow over the period. For the analysis of the stability, first, the discrete model of the system is derived and, then, by means of the Jacobian matrix or the Filippov's method [9], the stability is assessed. The evaluation of the stability is usually numerical but some papers have managed to derive stability criteria in a symbolic way [10, 11]. These stability criteria is for a converter with the slow loop opened, where the reference signal is constant rather than being controlled by a linear controller.

Unfortunately, when the loop is closed, the system usually tends to be more unstable. For example, an open-loop peak current-mode buck converter without a compensating ramp becomes unstable from a duty cycle greater than 50% but when the loop is closed, a sub-harmonic oscillation can appear for duty cycles less than 0.5. This is shown already in the Ridley current-mode model [4] but in most of the academic literature, the stability region without compensating ramp is still referred as $d < 0.5$. This results in a stability condition that does not represent the actual behavior of the closed-loop power converter. To derive a symbolic closed-loop stability criterion seems to be prohibitively complex in most cases. For example, a type-III controller will add three state variables. Furthermore, for the derivation of the symbolic discrete model the differential equation $\dot{x} = Ax + Bu$ needs to be solved in time-domain and, for the common approach, A needs to be invertible. Unfortunately, the inclusion of the state variables of a controller with a integral action will make the matrix A non invertible and, thus, a symbolic discrete map cannot be derived. El-Aroudi et al. [12] simplified a a closed-loop converter with a PI controller by considering only the proportional part as, at $f_{sw}/2$, is the one defining the stability. However, in ripple-based controls a pure integral type-I controller is usually used, so this approach is not valid.

Also, the inclusion of the ESL generates a problem that is illustrated in table I. The derivation of stability criteria using this method relies on the simplification $e^{AT} \simeq I + AT$ or $e^{AT} \simeq I + AT + \frac{1}{2}AT$ which usually works remarkable well for power converters. But table I shows for a 5 MHz buck converter, that when the ESL is considered, the simplification is very inaccurate. Therefore, a symbolic closed-loop modeling and stability criteria of $V^2 I_c$ using discrete modeling and Floquet theory is too complex and maybe not even feasible.

However, a simulation-based analysis based on the discrete modeling together with the Floquet theory can achieve extremely precise results in the modeling and the stability of the converter. This methodology can be easily implemented in commercial software and the intuitiveness of a transfer function or symbolic equations that can help to understand the system are lost in favor of high accuracy of the results and easy extension to other controls.

III. Floquet theory applied to power converters

The Floquet theory addresses the problem of determining the stability of periodic systems. The theory states that the periodicity of a periodic system can be maintained if the eigenvalues, called Floquet multipliers, of the monodromy matrix, ϕ_{cycle}, are all inside the unit circle. The monodromy matrix is the matrix that relates the perturbation at the beginning of a period and the perturbation at the end of that period $\triangle x(T) = \phi_{cycle} \cdot \triangle x(0)$. Consequently, the Floquet theory establishes whether a perturbation will grow over a period.

A. Monodromy matrix of hybrid systems

A hybrid system is a system that presents both continuous and discrete transitions. An example of such system is a piecewise smooth system that is of the form of

$$\frac{dx(t)}{dt} = \begin{cases} A_0 x(t) + B_0 u, & \text{if state 0} \\ \quad \ldots & \\ A_n x(t) + B_n u, & \text{if state n} \end{cases} \tag{1}$$

A model of this form can be easily derived for a power converter.

The monodromy matrix of hybrid systems is constructed by pre-multiplying transition matrices and saltation matrices [13]. Each of them takes into account the evolution of the perturbation during different times of the period:

- The transition matrix is the matrix that evaluates the evolution of a perturbation in a continuous system. In

TABLE I: Accuracy of the different approximations for the exponential of a matrix A_1T with and without considering the ESL.

	$\mathbf{A_1}$ (symbolic)	$e^{\mathbf{A_1T}}$	$\mathbf{I+A_1T}$	$\mathbf{I+A_1T+\frac{1}{2}A_1^2T^2}$
without ESL	$\begin{pmatrix} \frac{-1}{C(R+ESR)} & \frac{R}{C(R+ESR)} \\ \frac{-R}{L(R+ESR)} & \frac{-R\cdot ESR}{L(R+ESR)} \end{pmatrix}$	$\begin{pmatrix} 0.94 & 0.04 \\ -1.93 & 0.95 \end{pmatrix}$	$\begin{pmatrix} 0.97 & 0.04 \\ -1.99 & 1 \end{pmatrix}$	$\begin{pmatrix} 0.93 & 0.04 \\ -1.96 & 0.95 \end{pmatrix}$
with ESL	$\begin{pmatrix} 0 & 0 & \frac{1}{C} \\ 0 & \frac{-R}{L} & \frac{R}{L} \\ \frac{-1}{ESL} & \frac{R}{ESL} & \frac{-(R+ESR}{ESL} \end{pmatrix}$	$\begin{pmatrix} 0.94 & 0.04 & 0 \\ -1.92 & 0.95 & 0004 \\ -2.53 & 0.92 & 0.004 \end{pmatrix}$	$\begin{pmatrix} 1 & 0 & 0.04 \\ 0 & -2 & 3 \\ -500 & 750 & -751.5 \end{pmatrix}$	$\begin{pmatrix} -9 & 15 & -15.01 \\ -750 & 1127.5 & -1130.2 \\ 187620 & -282560 & 283490 \end{pmatrix}$

case the system evolves from $t = 0$ to $t = dT$ in state i ($dx(t)/dt = A_i x(t) + B_i u$), then the transition matrix is $\phi_i(dT) = e^{A_i t}$.

- The saltation matrix [13], [14] is the matrix that evaluates the evolution of the perturbation across a switching hyper-surface. A switching hyper-surface is the mathematical form of the condition for jumping from state i to state j and, in power converters, it is commonly of the form of

$$h(x(t), t) = Kx(t) + Gu + m(t) \tag{2}$$

where the condition to commutate the switches depends on the state variables, the input and an external time-varying signal, for example, a ramp.
The saltation matrix [14] is obtained from the formula:

$$S = I + \frac{(f_{p+} - f_{p-})n^T}{n^T f_{p-} + \frac{\partial h}{\partial t}(t_p, x(t_p))} \tag{3}$$

where I is the identity matrix, f_{p-} is the differential state dx/dt just before the switching, f_{p+} is the differential state dx/dt just after the switching and n is the normal to the hyper-surface $h(x(t), t)$ ($n = K$ if (2) applies).
Note that when the switching is forced (as in controls using a latch RS), the switching condition is not an actual hyper-surface and, therefore, the term n of the equation (3) is a vector of zeros and, therefore, the saltation matrix at that instant is the identity matrix.

To build the monodromy matrix, the "path" traveled by the perturbation needs to be followed. For a system that starts in state 1, then at $t = t_1$, it switches to state 0 and continues in that state until it switches back at $t = t_2$ to state 1 (fig.3), the monodromy matrix is:

$$\phi_{cycle} = S_0(t_2) \cdot e^{A_0 \cdot (t_2 - t_1)} \cdot S_1(t_1) \cdot e^{A_1 \cdot t_1} \tag{4}$$

This expression takes into account the overall evolution of the perturbation. The evolution during state 1 is the transition matrix $e^{A_1 \cdot (t_1)}$, the evolution across the first switching is the saltation matrix $S_1(t_1)$, the evolution during state 0 is the transition matrix $e^{A_0 \cdot (t_2 - t_1)}$ and the evolution across the second switching is the saltation matrix $S_0(t_2)$.

IV. V^2I_c CONTROL OF A BUCK CONVERTER AND ITS MATHEMATICAL MODEL

This section explains the discrete modeling of the V^2I_c control[1] (fig.4). The V^2I_c control is proposed to optimize the dynamic response of buck converters. It provides very fast transient responses under voltage reference steps and load steps. The control presents an inner fast loop where the current through the capacitor, the output voltage and a compensating ramp to stabilize the system are added. In the outer slow loop, the error of the output voltage passes through a linear controller. The PWM modulation is made using a latch RS and a clock signal to provide fixed switching frequency. Fig.4 shows an electrical model of the V^2I_c control with all the considered parasitic elements. The ON-resistance of the switches R_1 and R_0, the resistance of the inductor, R_L, the ESR, and the ESL of the output capacitor are the parasitic elements of the power stage. The compensating ramp, v_{ramp} is modeled over a period T as $v_{ramp}(t) = m_{ramp} \cdot t + H$ where m_{ramp} is the slope of the ramp and H is the offset voltage. The peak-to-peak amplitude of the ramp is $V_{pp} = m_{ramp} \cdot T$.

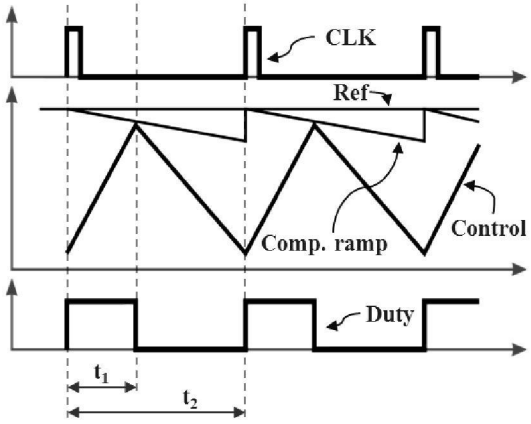

Fig. 3: Switching diagram of V^2I_c control.

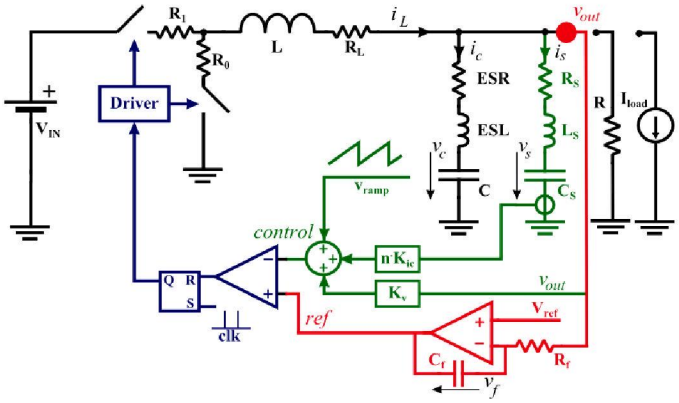

Fig. 4: Electrical scheme of a V^2I_c controlled buck converter.

The linear regulator is a type-I controller with resistance R_f and capacitor C_f. The gain of the error of the output voltage is K_v.

A. Measurement of the current through the output capacitor

The current through the output capacitor is measured by adding a parallel RLC network [2]. The actual implementation is done by means of a trans-impedance amplifier but, for the analysis of the control, it is sufficient to consider only the equivalent parallel RLC network (fig.2). For a correct measurement of the current, the impedance of the parallel network must be proportional to the impedance of the output capacitor, $Z_{C_{out}} = n \cdot Z_{RLC}$, where n is the gain of the current sensor:

$$C_s = C/n;\ R_s = n \cdot ESR;\ L_s = n \cdot ESL \tag{5}$$

When these conditions are fulfilled, the current through the parallel network is $1/n$ times the current through the output capacitor

$$i_s = i_c/n \tag{6}$$

The measurement of the output capacitor current is, then, weighted with a gain K_{ic}.

B. Piece-wise smooth model of the system

The state variables, x, of the system are the voltage in the output capacitance, v_c, the voltage in the capacitance of the parallel network, v_s, the current through the inductor, i_L, the current through the output capacitor, i_c, the current through the parallel network, i_s, and the voltage in the capacitor of the regulator, v_f:

$$x(t) = \big(v_c(t),\ v_s(t),\ i_L(t),\ i_c(t),\ i_s(t),\ v_f(t)\big)^T \tag{7}$$

The input variables, u, are the input voltage, V_{in}, the reference voltage, V_{ref}, and current demanded by the load, I_{load}:

$$u = (V_{in},\ V_{ref},\ I_{load})^T \tag{8}$$

The general form of a piece-wise smooth model is shown in (1). For $V^2 I_c$ control, it is of the form:

$$\frac{dx(t)}{dt} = \begin{cases} A_0 x(t) + B_0 u, & \text{if state 0} \\ A_1 x(t) + B_1 u, & \text{if state 1} \end{cases} \tag{9}$$

where the state 1 is when the high-side MOSFET of the buck converter is conducting and the state 0 is when the low-side MOSFET is conducting.

The switching hyper-surface that takes into account the switching from state 1 to state 0 is the intersection of the control signal with the reference signal (fig.3). It is of the form of:

$$h_{10}(x,t) = Kx(t) + Gu + m_{ramp}t + H \tag{10}$$

Due to the integral action of the closed-loop control, the matrices A_0 and A_1 are non invertible. Then, the solution of the differential equation $dx(t)/dt = Ax(t) + Bu$, needed for the derivation of the discrete model, cannot be directly solved, and rather, another approach is needed.

The augmented state-vector [15] provides an elegant method to solve the problem by creating a new variable vector, y, that is composed by the state variables (7) and the input variables (8):

$$y(t) = \big(v_c(t), v_s(t), i_L(t), i_c(t), i_s(t), v_f(t), V_{in}, V_{ref}, I_{load}\big)^T \tag{11}$$

In this way, the system can be defined as:

$$\frac{dy(t)}{dt} = \begin{cases} \hat{A}_0 y(t), & \text{if state 0} \\ \hat{A}_1 y(t), & \text{if state 1} \end{cases} \tag{12}$$

where

$$\hat{A}_0 = \begin{pmatrix} A_0 & B_0 \\ 0 & 0 \end{pmatrix}; \qquad \hat{A}_1 = \begin{pmatrix} A_1 & B_1 \\ 0 & 0 \end{pmatrix} \tag{13}$$

The switching hyper-surface that takes into account the switching from state 1 to state 0 is:

$$h_{10}(y,t) = \hat{K} y(t) + m_{ramp}t + H \tag{14}$$

where

$$\hat{K} = (K,\ G) \tag{15}$$

C. Discrete model of the system

The discrete model of the system is a function or collection of functions that relate the state variables at the beginning of a period with the state variables at the end of that period.

Let T be the switching period of the control and the sample period of the discrete model. Let the initial state, y_k, be the value of the variables of the vector $y(t)$ at the beginning of the period and let the final state, y_{k+1}, be the value of the variables of the vector y at the end of the period. Let d be the duty cycle, where $t = dT$ is the time at which the converter changes to state 0. Then, after solving (12) as a time-domain model and combining it with the switching hypersurface (10), the large-signal closed-loop implicit discrete model of the converter is derived:

$$y_{k+1} = f(y_k, d); \qquad g(y_k, d) = 0 \tag{16}$$

where

$$g(y_k, d) = \hat{K} \cdot e^{\hat{A}_1 dT} y_k + m_{ramp} dT + H = 0 \tag{17}$$

and

$$y_{k+1} = e^{\hat{A}_0 (1-d)T} \cdot e^{\hat{A}_1 dT} \cdot y_k \tag{18}$$

Normally, this model would be explicit, where the duty cycle can be obtained as an explicit function of the initial state, but this is achieved by simplifying the exponential term of eq. (17) by its first or second Taylor expansions. However, when the ESL of the output capacitor is included in the model, this simplification is not valid (see table I) and therefore the function that relates the initial state and the duty cycle is implicit.

Note that the discrete model is *not* a discrete transfer function $G(z)$. The derived discrete model is nonlinear and presents no simplifications. Furthermore, the complete time-domain model can be derived from the discrete model (16). In the paper, the figures labeled with discrete modeling use this

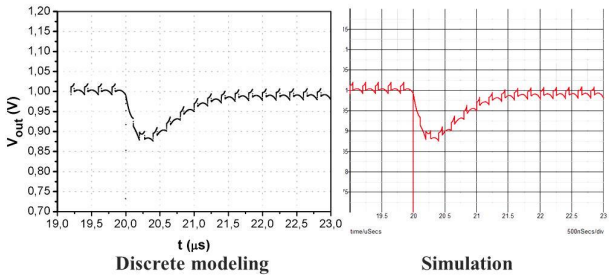

(a) Output voltage.

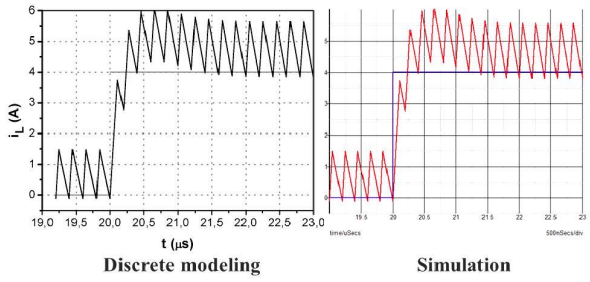

(b) Inductor current.

Fig. 5: Comparison between the discrete model (left) and simulation results from Simplis (right) under a load step $0A \rightarrow 4A$.

time-domain solution to plot the ripple of the signals.

Figure 5 validates the goodness of the model by comparing the discrete model derived including the ripple and simulation results from the program *Simplis*. The dynamic behavior and the ripple of the signals are in agreement.

V. Stability analysis of V^2I_c

This section shows the stability analysis of the V^2I_c control using the Floquet theory. The Filippov's method is employed to find out the monodromy matrix.

A. Filippov's method

Equation (4) shows the expression of the monodromy matrix using the Filippov's method. The saltation matrix corresponding to the first switching, that occurs at $t = dT$ is:

$$S_1(dT) = I + \frac{(f_{dT+} - f_{dT-})n^T}{n^T f_{dT-} + \dfrac{\partial h}{\partial t}(dT, x(dT))} \qquad (19)$$

where $f_{dT+} = A_0 x(dT) + B_0 u$, $f_{dT-} = A_1 x(dT) + B_1 u$, $n = K$ and $\partial h/\partial t(dT, x((dT)) = m_{ramp}$.

The monodromy matrix is:

$$\phi_{cycle} = e^{A_0(1-d)T} \cdot S_1(dT) \cdot e^{A_1 dT} \qquad (20)$$

If all the eigenvalues, called Floquet multipliers, are in the open unit disk, the system is locally asymptotically stable.

Fig.6 shows a comparison between the bifurcation diagram obtained from the discrete model and the stability analysis, showing a complete agreement that validates the method at

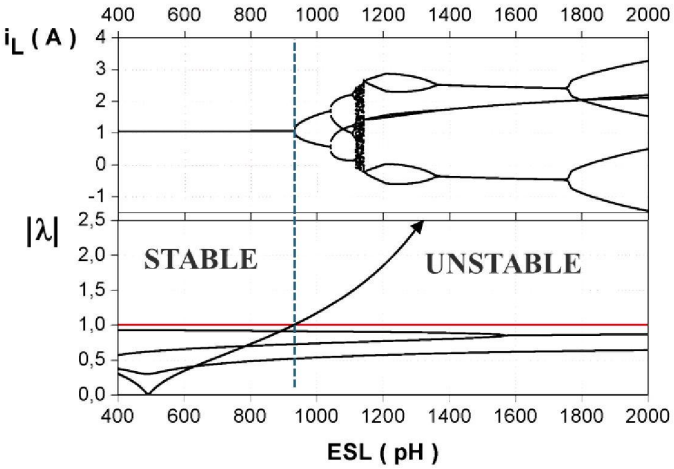

Fig. 6: Comparison of the bifurcation diagrams and the stability analysis varying the ESL (sensor designed for $ESL_n = 444pH$. Upper part: inductor current sampled every T seconds. Lower part of (a) and (b): module of the eigenvalues.

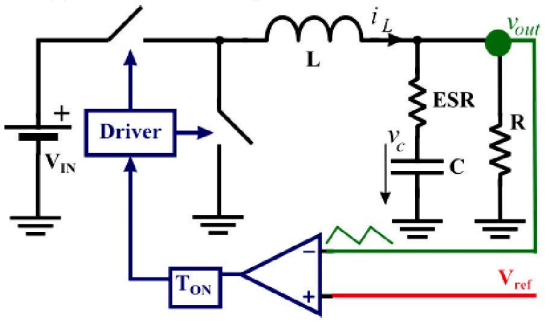

Fig. 7: Open-loop V^2 current mode with constant T_{on}.

simulation level. When varying the ESL of the output capacitor or the compensating ramp, the system becomes unstable at the same moment that an eigenvalue goes out of the open unit disk.

VI. Sensitivity analysis of ripple-based controllers

The combination of discrete modeling and Floquet theory allows the derivation of powerful tools: as critical parameters of the power converter are varied, the required values of the state variables are retrieved from the discrete modeling and the Filippov's method is employed to find out the Floquet multipliers and establish stable region diagrams. In this section, the proposed method is applied to a buck converter with different ripple-based controllers: V^2I_c control , V^2 with constant T_{on} [5] (fig.7) and V^2 with constant switching frequency [16] (fig.8).

A. Sensitivity analysis of V^2I_c

Several parameters are to be considered to perform a full sensitivity analysis of the V^2I_c control. Sub-harmonic oscillations and stability issues depend on the range of the duty cycle operation, gain of the capacitor current loop, slope of the compensating ramp, variation of the ESL of the output capacitor and mismatches of the current sensor. The proposed sensitivity analysis based on Floquet theory accounts for

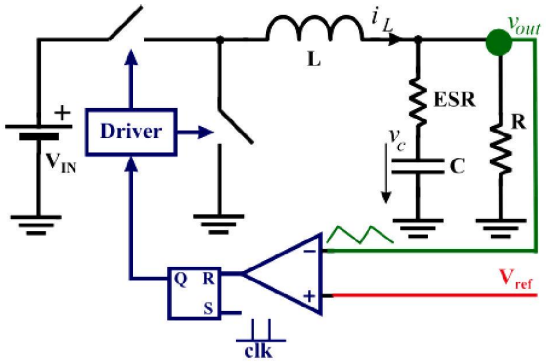

Fig. 8: Open-loop V^2 current mode with fixed switching frequency.

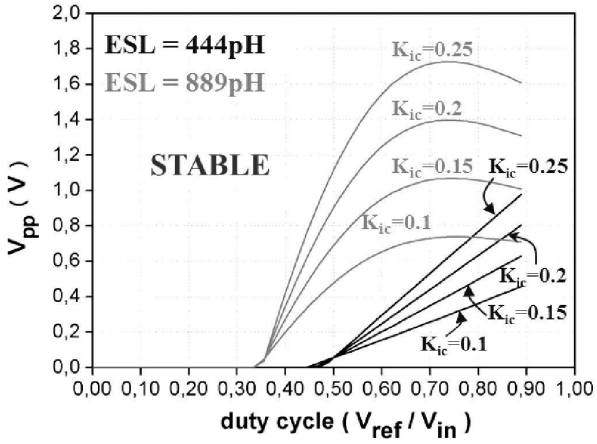

Fig. 9: Sensitivity analysis of $V^2 I_c$. It shows the required compensating ramp for different duty cycles, ESL and gain of the current loop. The stable regions are the upper area of the curves. Sensor designed for $ESL_n = 444pH$.

all these parameters. The parameters of the converter are: $V_{in} = 4.5V$, $V_{out} = 1V$, $I_{load} = 0A$, $R = 1.8\Omega$, $L = 100nH$, $R_L = 10m\Omega$, $R_1 = R_0 = 50m\Omega$, $C = 4\mu F$, $ESR = 4.5m\Omega$, $ESL = 444pH$, $K_i = 1/(R_f C_f) = 3.7 \cdot 10^5$, $K_v = 1$. The current sensor is initially well-designed with a gain of $n = 1000$: $C_s = C/n$, $R_s = nESR$, $L_s = nESL$. Fig.9 shows the sensitivity analysis by means of stable region diagrams.

B. Sensitivity analysis of V^2 with constant T_{on}

V^2 control is a well-known technique. When the ESR of the output capacitor is dominant, the ripple of the output voltage presents a triangular shape due to the voltage drop in the ESR and enables a ripple-based controller using the output voltage as the triangular reference signal. The control, then, relies on the assumption of the triangular shape of the output voltage and, thus, a switching frequency or ESR too low may lead to a sub-harmonic oscillation. The Describing Function technique [5] manages to derive a control-to-output transfer function, where the following condition for stability is achieved after simplifying:

$$\text{Stable when } T_{on}/2 < ESR \cdot C \tag{21}$$

This is the same stability criterion obtained from the discrete model derived in [11].

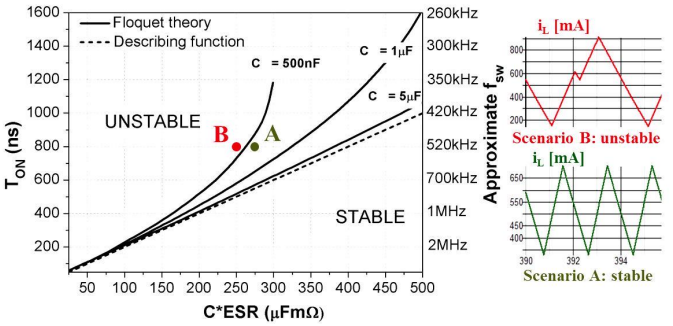

Fig. 10: Stable region diagram varying constant T_{on}, capacitance C and ESR of the output capacitor. Sensitivity analysis of V^2, constant T_{on}. The stability analysis is verified at simulation level. Simulated inductor current waveforms. $T_{on} = 800ns$. Scenario A (stable): $C = 500nF$, $ESR = 540m\Omega$. Scenario B (unstable): $C = 500nF$, $ESR = 500m\Omega$.

This control technique is analyzed using an accurate discrete modeling and Floquet theory. The parameters of the converter are $V_{in} = 12V$, $V_{out} = 5V$, $L = 15\mu H$ and $R = 10\Omega$. Fig.10 shows the sensitivity analysis using the Describing Function and the Floquet theory varying the constant T_{on} and the ESR and capacitance C of the output capacitor. The Describing Function is more conservative and the Floquet theory is more accurate and allows for a smaller capacitor or lower switching frequency. Also, varying the output capacitor while remaining constant the product $C \cdot ESR$ has a critical effect on stability: decreasing the output capacitor greatly stabilizes the circuit for low frequencies and high product $C \cdot ESR$. This behavior is not predicted by the stability criterion derived from Describing Function.

For a technology of capacitors with a product $C \cdot ESR = 250\mu F \cdot m\Omega$, the minimum switching frequency for stability is $570kHz$ for an output capacitor of $500nF$, $720kHz$ for $C = 1\mu F$ and $810kHz$ for $C = 5\mu F$. The stability criterion derived from the Describing Function model wrongly states that the minimum switching frequency is $840kHz$, independently of the capacitance of C.

C. Sensitivity analysis of fixed frequency V^2

V^2 control can be modulated also with a fixed frequency PWM. For this case, the stability condition [16] is:

$$F_{sw} \geq \frac{1}{C \cdot ESR} \cdot \left(\frac{1}{2} + \frac{D^2}{1-2D}\right) \tag{22}$$

This is, again, the same stability criterion obtained from the discrete model derived in [11].

Figure 11 shows the sensitivity analysis using the Describing Function and the Floquet theory for a duty cycle of 0.4. For the Describing Function, the minimum switching frequency is only dependant on the product $C \cdot ESR$ and the duty cycle. The comparison shows that the Floquet theory is more accurate for high ESR capacitors and low capacitance. Also, figure 12 compares the stability condition derived from Describing Function of the open-loop system with the stability criterion from the Floquet theory of the closed-loop system compensated with a type-I controller where the unity gain of

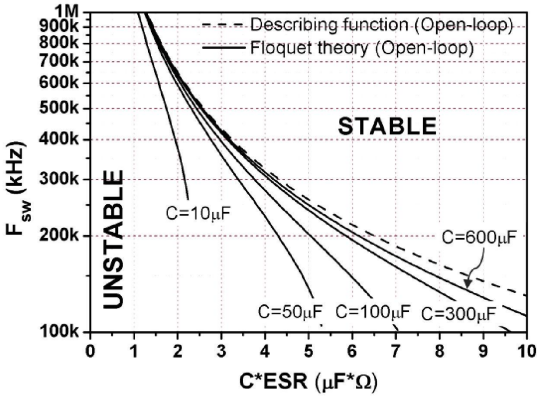

Fig. 11: Sensitivity analysis of open-loop fixed-frequency V^2 with $D = 0.4$. The stable region is the upper area of the proper curve. Describing Function does not fully represent the system behaviour.

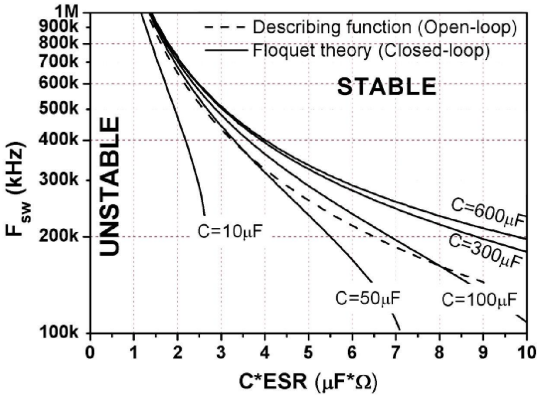

Fig. 12: Sensitivity analysis of closed-loop fixed-frequency V^2 with $D = 0.4$. The stable region is the upper area of the proper curve. The open-loop stability criterion does not fully represent the closed-loop system behavior.

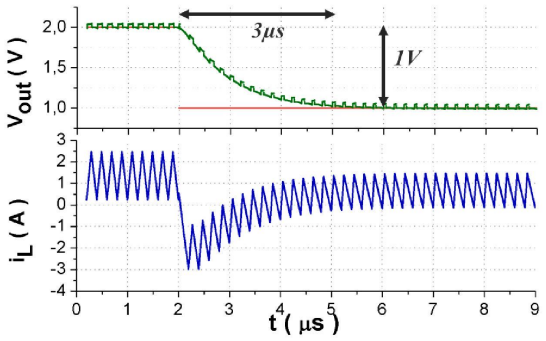

(a) Discrete modeling: Negative voltage reference step of 1 V from 2 V to 1 V, output voltage in green (500 mV/div), voltage reference in orange (250 mV/div), inductor current in blue (1 A/div) with $1\mu s/div$ time scale.

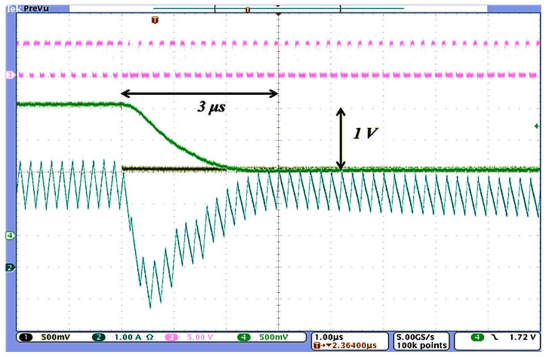

(b) Experimental results: Negative voltage reference step of 1 V from 2 V to 1 V, output voltage in green (500 mV/div), voltage reference in yellow (500 mV/div), inductor current in blue (1 A/div), (b) measured current in purple (500 mV/div) and gate signal in purple (5 V/div) with $1\mu s/div$ time scale.

Fig. 13: Experimental validation of discrete modeling.

the controller is at 100 kHz. It shows that, when the loop is closed, sub-harmonic oscillations appear before in the system and the open-loop stability criterion falls short.

VII. Experimental results

This section documents the stability analysis of the V^2I_c control. The experimental prototype is designed according to the sensitivity analysis of the section VI.

The experimental system switches at a frequency of $5\ MHz$. The input voltage V_{in} is $4.5V$ and the nominal output voltage V_{out} is $1V$. The parameters of the power stage are: $R_1 = R_0 = 40m\Omega$, $L = 100nH$, $R_L = 10m\Omega$, $C = 4\mu F$, $ESR = 4.86m\Omega$, $ESL = 1.2nH$. For a well-designed sensor: $C_s = 4nF$, $R_S = 4.86\Omega$, $L_s = 1.2\mu H$. The parameters of the control are: $f_{sw} = 5MHz$, $d_{min} = 5\%$, $d_{max} = 95\%$, $V_{pp} = m_{ramp}/T = 0.37V$, $K_{ic} = 0.245$, $K_v = 1$, $R_f = 1k\Omega$, $C_f = 2.42nF$.

A. Validation of discrete modeling

The discrete modeling of the system is validated by comparing the dynamic behavior of the modeling under a voltage reference step with the experimental behavior measured in the prototype.

The system is plotted under a negative voltage reference step of $2\ V \rightarrow 1\ V$ (fig.13).

The dynamic behavior of the discrete model and the experimental prototype greatly agree.

B. Validation of analysis of local stability

The previous parameters remain the same except the ramp, which is set to an amplitude of $0.37V$ in order to provoke an instability.

The Floquet theory predicts that the system becomes unstable from an output voltage of $3.1V$ (fig.14): for $V_{out} = 3V$, all Floquet multipliers remain inside the unit circle, but one of them is in the border at -0.9654. When the output voltage is increased to $3.1V$, that multiplier is -1.064, and thus, gets out of the unit circle. Floquet theory states, then, that the converter is unstable at $V_{out} = 3.1V$.

This prediction is validated experimentally (fig.15). The converter becomes unstable at the very same point predicted by the analysis, resulting in a very precise method to predict instabilities.

Note that the reference signal $v_{reference}$ (yellow signal), which is the output of the linear controller, does not change, meaning that the slow loop is unaware of the oscillation in the fast loop.

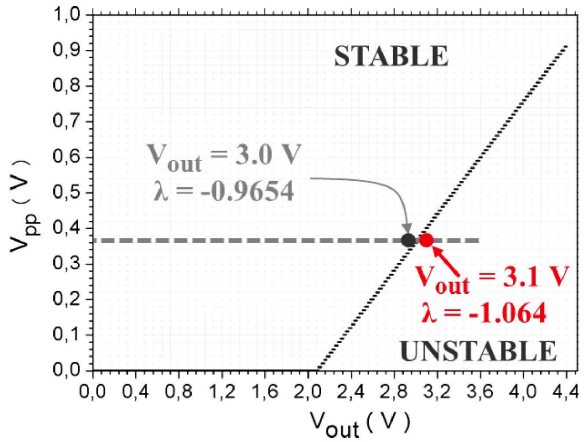

Fig. 14: Stable region diagram varying compensating ramp and output voltage. The eigenvalues and the output voltages at the border of stability are shown for a ramp with an amplitude voltage of $V_{pp} = 0.37V$.

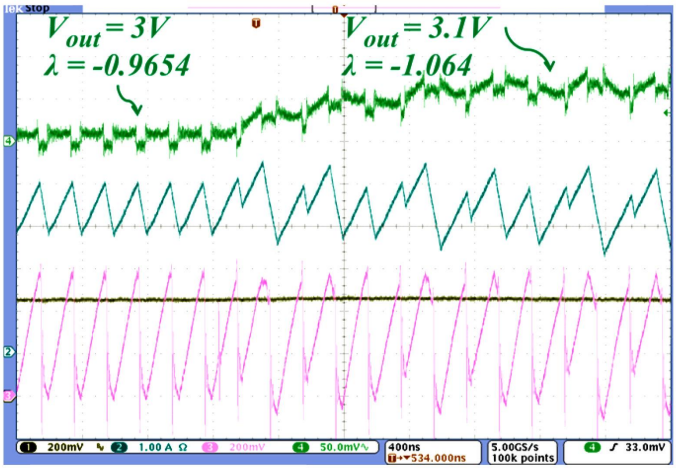

Fig. 15: Experimental results: positive voltage reference step of $0.1\ V$ from $3\ V$ to $3.1\ V$, output voltage in green (AC coupling, $50\ mV/div$), inductor current in blue ($1\ A/div$), control signal $v_{control}$ in purple ($200\ mV/div$) and reference signal $v_{reference}$ in yellow ($200\ mV/div$) with $400ns/div$ time scale.

VIII. Conclusion

V^2I_c control was modeled and analyzed using a simulation-based discrete modeling and Floquet theory. The discrete model provides the large-signal behavior of the converter with the possibility of simulating the time-domain waveforms (figures 5 and 13). The Floquet theory predicts with extreme precision sub-harmonic oscillations of the power converter. Figures 14 and 15 show the experimental validation of the stability analysis by predicting for a buck converter with V^2I_c control that an increase of $100mV$ of an output voltage of $3V$ will lead to an instability. The methodology is extended to different V^2 architectures. A comparison with the stability criterion derived with the Describing Function shows that the Floquet theory predicts more accurately and the Describing Function is too conservative for converters with low switching frequency or high ESR of the output capacitor.(fig.10 and 11). Also, figure 12 shows that the stability criterion derived from an open-loop system falls short because the system tends to be more unstable when the loop is closed.